Dynamics of *Deinococcus radiodurans* under Controlled Growth Conditions

Sidhartha S. Jena,* Hiren M. Joshi,† K. P. V. Sabareesh,* B. V. R. Tata,* and T. S. Rao†
*Materials Science Division, Indira Gandhi Center for Atomic Research, Kalpakkam 603 102, Tamil Nadu, India;
and †Water and Steam Chemistry Division, Bhabha Atomic Research Center Facilities, Kalpakkam 603 102, Tamil Nadu, India

ABSTRACT *Deinococcus radiodurans* is a potent radiation resistant bacterium with immense potential in nuclear waste treatment. In this investigation, the translational and rotational dynamics of dilute suspensions of *D. radiodurans* cultured under controlled growth conditions was studied by the polarized and depolarized dynamic light-scattering (DLS) techniques. Additionally, confocal laser scanning microscopy was used for characterizing the cultured samples and also for identification of *D. radiodurans* dimer, tetramer, and multimer morphologies. The data obtained showed translational diffusion coefficients (D_T) of 1.2×10^{-9}, 1.97×10^{-9}, and 2.12×10^{-9} cm^2 /s, corresponding to an average size of 3.61, 2.22, and 2.06 μm, respectively, for live multimer, tetramer, and dimer forms of *D. radiodurans*. Depolarized DLS experiments showed very slow rotational diffusion coefficients (D_R) of 0.182/s for dimer and 0.098/s for tetramer morphologies. No measurable rotational diffusion was observed for multimer form. Polarized DLS measurements on live *D. radiodurans* confirmed that the bacterium is nonmotile in nature. The dynamics of the dead dimer and tetramer *D. radiodurans* were also studied using polarized and depolarized DLS experiments and compared with the dynamics of live species. The dead cells were slightly smaller in size when compared to the live cells. However, no additional information could be obtained for dead cells from the polarized and depolarized dynamic light-scattering studies.

INTRODUCTION

Light scattering measurements have found many applications in biology, ranging from the assessment of bacterial concentration in a suspension to the resolution of the fine structure of the cells and also to determine the size and shape of the molecules (1). Among the various methods, dynamic light scattering (DLS) is one of the most powerful techniques used extensively for studying the dynamics of macromolecules in solutions/suspensions. This technique basically deals with particles, which undergo Brownian motion in the solutions. The average translational motion of particles depends on the particle size, thermal energy, viscosity of the medium, and particle geometry. Conventional DLS (2) probes the translational motion of the particles, from which information about the particles dimensions can be obtained, whereas depolarized dynamic light scattering (3) (DDLS) probes both the rotational and translational motion of the particles. The depolarized component of the scattered light is produced either by geometrically or optically anisotropic particles. The depolarized DLS can provide information about the shape of the particles along with its dimensions. The depolarized DLS experiment is also much more sensitive to small changes in particle size, because of a much stronger size (d) dependence of ($1/d^3$) compared to the ($1/d$) dependence for DLS. Confocal laser scanning microscopy is another technique, where imaging is used to study large particles with respect to the particle size and shape. DLS, DDLS combining with confocal microscopy can be used to study the dynamics of macromolecules, vis-à-vis can be applied to bacteria.

Managing nuclear waste is one of the challenges faced by the nuclear industry worldwide (4,5). Among several physicochemical technologies used for the treatment of active waste, bioremediation is developing as an alternative technology (6). We have applied DLS, DDLS, and confocal microscopy to study the dynamics of *Deinococcus radiodurans*, a bacterium that can resist up to 18 KGy of radiation dose and is emerging as a promising candidate for bioremediation of nuclear waste (7,8). *D. radiodurans* can be isolated from locations rich in organic nutrients like; soil, animal feces, and processed meats, as well as from dry and nutrient poor environments (9,10). Tremendous effort has been made by several groups to understand the radiation resistance of this bacterium (11,12). The common morphology of *D. radiodurans* bacteria cells is tetrameric (13,14). This bacterium grows and divides in a dimer/tetramer (designated as 2/4) fashion under normal growth conditions (14). *D. radiodurans* has extraordinary resistance to the lethal and mutagenic effects of many DNA damaging agents, viz. ultraviolet, ionizing radiation, and chemical mutagens. All the strains of this genus are radiation and desiccation resistant (12). This unusual bacterium survives in extreme conditions of environments because of its ability to repair damaged DNA quickly (12). Studies on varied morphologies (dimer, tetramer, and multimer) of *D. radiodurans* have lot of relevance in their mode of growth on different substrates (which aids in better understanding of the biofilm formation property) with respect to surface decontamination. Moreover,

Submitted April 5, 2006, and accepted for publication June 16, 2006.

Address reprint requests to Dr. Sidhartha S. Jena, Materials Science Division, Indira Gandhi Center for Atomic Research, Kalpakkam 603 102, Tamil Nadu, India. Tel.: 91-44-27480347; Fax: 91-44-27480081 or 91-44-27480301; E-mail: sid@igcar.gov.in.

0006-3495/06/10/2699/09 $2.00

doi: 10.1529/biophysj.106.086520

morphological variants can show disparate radiation resistance property. Also, the different forms of this bacterium can aid in better gene manipulation, thereby enhancing the bioremediation potential of this bacteria.

Inspired by the extraordinary properties of this bacterium, we have successfully grown *D. radiodurans* cultures with predominantly dimer, tetramer, and multimer forms, using controlled growth conditions. To the best of our knowledge, this is the first time *D. radioduran* bacterium with predominantly dimer and multimer forms were cultured under a controlled nutrient condition. It is important to characterize the grown culture of *D. radiodurans* for a), their predominance of a particular form, and for b), their size and shape relationship with change in morphologies. Further, we are also interested in verifying the motility of the live bacteria cells. DLS is the appropriate tool for characterizing these quantities of the microorganism. Hence, we employ both polarized and depolarized DLS technique for measuring the translational and rotational diffusion coefficients of *D. radiodurans* of different morphologies in dilute suspensions as well as the motility of the live *D. radiodurans* cells. The measurement of translational and rotational diffusion coefficient of different forms of *D. radiodurans* can provide an insight into dissimilarities in their size and shape. Additional information about the predominance of a particular form in respective culture samples can be obtained via polydispersity index parameter. We also confirm the results of DLS data by performing fluorescence confocal laser scanning microscopy on the cultured samples. Further, we report polarized and depolarized DLS results on the dead dimer and tetramer samples of *D. radiodurans* to differentiate any change in dynamics with that of the live samples.

MATERIALS AND METHODS

Bacterial culture

D. radiodurans R1 (B2906, NRRLB) was cultured in TGY (tryptone 1.0%, glucose 0.1%, yeast extract 0.5%) medium and incubated at 37°C for 24 h. This culture medium and conditions lead to the formation of the multimer form of *D. radiodurans*. By using a similar procedure with controlled growth conditions, i.e., primarily by varying the nutrient concentration, we could culture predominantly dimer and tetramer forms of the bacterium. After the growth, the *D. radiodurans* culture was centrifuged at 8000 rpm in a refrigerated centrifuge. The cell pellet obtained was washed twice in ultrapure phosphate saline buffer (PBS) to remove any debris.

For DLS measurements, the pellet was further washed twice with 0.2 μm filtered PBS buffer. The washed pellet was resuspended directly into the light-scattering cell (quartz) of 8 mm inner diameter with 1 ml of ultra-filtered PBS buffer. Further dilutions were made with the same ultra-filtered buffer to the required concentrations before DLS measurements were carried out.

Confocal microscopy

The confocal microscopy (15) measurements on *D. radiodurans* cells were performed using Leica TCS-SP2-RS (Wetzlar, Germany) confocal laser scanning microscope (CLSM) system operating in fluorescence mode. The CLSM is interfaced with a Leica DMIRE2 inverted microscope and the images were taken using a 63×/1.2 numerical aperture, water immersed objective lens. The *D. radiodurans* cells are stained with acridine orange and excited using an Ar^+ ion laser operating at 488 nm. The emitted fluorescence signal was collected with a wavelength window of 500–550 nm using a photo multiplier tube (PMT) for imaging the bacteria cells. For these experiments, 50 μl of *D. radiodurans* suspension was spread on to a glass slide and air-dried. The smear was stained with 20 μl of 0.02% of acridine orange (absorption maximum ~490 nm, emission maximum ~520 nm) for a few minutes. Excess stain was washed with ultra-pure water, and the stained sample was air-dried. A thin coverslip was placed on the smear and the slide was mounted on to the microscope stage for observation using CLSM. Acridine orange is an intercalating dye that binds to the double-stranded DNA inside the bacteria cells, and these dye-tagged molecules of double-stranded DNA emit fluorescence signal in green (16) when excited with an Ar^+ ion laser operating at 488 nm, and helps in imaging the *D. radiodurans* cells. Dead bacteria were confirmed after staining with live/dead staining technique (Molecular Probes, Eugene, OR), wherein the dead cells fluoresce red. All the images were taken by scanning a frame of 512 × 512 pixels with the laser beam in the x, y plane, and each image was averaged over 40 frames for a better signal/noise ratio.

Dynamic light scattering

Polarized (VV, vertical/vertical) and depolarized (VH, vertical/horizontal) DLS measurements on dilute suspensions of *D. radiodurans* were performed using a Malvern 4700 (Malvern Instruments, Malvern, UK) light-scattering setup equipped with a Malvern made goniometer, a multi-tau correlator, and a 2.5 W (Ar^+ + Kr^+) ion laser (Spectra-Physics (Mountain View, CA), model No. 2018-RM) operating at 514.5 nm. For polarized and depolarized DLS measurements, the incident laser beam was vertically polarized and the scattered intensity was collected using a Glan-Thompson prism (Melles Griot, Rochester, NY), placed in front of the PMT in the vertical and horizontal polarization respectively. The normalized intensity-intensity autocorrelation function (ICF), $g^{(2)}(q,\tau)$measured directly using a multi-tau correlator at a given scattering wave vector, $q = (4\pi n/\lambda)\sin(\theta/2)$ is given by (2),

$$g^{(2)}(q,\tau) = \frac{\langle I(q,t)I(q,t+\tau)\rangle}{\langle I(q,t)\rangle^2}, \tag{1}$$

where n is the refractive index of the medium, λ is the wavelength of the incident laser beam, and θ is the scattering angle.

For a scattered electric field obeying Gaussian statistics, the ICF is related to $g^{(1)}(q,\tau)$, the normalized electric field correlation function, $\langle E^*(q,t+\tau)E(q,t)\rangle/|\langle E(q,t)\rangle|^2$by the Siegert relation (17)

$$g^{(2)}(q,\tau) = 1 + f|g^{(1)}(q,\tau)|^2, \tag{2}$$

where f is an instrumental parameter $0 < f < 1$,related to the spatial coherence (2). In general, the field correlation function, $g^{(1)}(q,\tau)$, can be expressed as a distribution function of decay rates Γ,

$$|g^{(1)}(q,\tau)| = \int_0^\infty G(\Gamma)\exp(-\Gamma\tau)d\Gamma, \tag{3}$$

where $G(\Gamma)d\Gamma$ is the contribution to the total scattering from the decay process with decay constants between Γ and $\Gamma+d\Gamma$. The form of $g^{(1)}(q,\tau)$ depends on the system under study and for a dilute solution of monodispersed particles, it can be represented by a single exponential,

$$g^{(1)}(q,\tau) = \exp(-\Gamma\tau), \tag{4}$$

where Γ is the decay constant related to translational diffusion coefficient by, $\Gamma = Dq^2$.

In the case of isotropic particles, translational motion alone contributes to the field correlation function, $g^{(1)}(q,\tau)$. For a dilute solution of spherical, monodispersed, and optically isotropic particles, $g^{(1)}(q,\tau)$ can be described by Eq. 4, whereas in the case of geometrically or optically anisotropic

particles, both translational and rotational motions contribute to the correlation function, $g^{(1)}(q,\tau)$. Anisotropic particles depolarize the incident light, and the scattered electric field can be decomposed into parallel and perpendicular components with respect to the incident polarization. The polarized electric field correlation function, $g^{(1)}_{VV}(q,\tau)$, in its normalized form can be written as (18,2)

$$g^{(1)}_{\mathrm{VV}}(q,\tau) = \frac{45\alpha^2}{(45\alpha^2+4\beta^2)}\exp(-q^2D_{\mathrm{T}}\tau) + \frac{4\beta^2}{(45\alpha^2+4\beta^2)}\exp[-(q^2D_{\mathrm{T}}+6D_{\mathrm{R}})\tau] \quad (5)$$

and the depolarized electric field correlation function, $g^{(1)}_{\mathrm{VH}}(q,\tau)$,in its normalized form can be written as (18,2)

$$g^{(1)}_{\mathrm{VH}}(q,\tau) = \exp[-(q^2D_{\mathrm{T}}+6D_{\mathrm{R}})\tau], \quad (6)$$

where D_{T} andD_{R} are the translational and rotational diffusion coefficients, respectively, and α, β are the isotropic and anisotropic parts of the polarizibility tensor respectively. For large rod-shaped particles ($qL > 5$), more exponential terms containing both translational and rotational diffusion coefficients should be added (19) to Eqs. 5 and 6. But these additional terms, including the second term on the right-hand side of Eq. 5, are negligible in the limit of $qL \rightarrow 0$ or for spherical particles. In the study presented here, although all forms of *D. radiodurans* are large in size, their aspect ratio is quite small and also is not rigid in nature. Hence all forms of *D. radiodurans* can be approximated to nearly spherical in shape. This can be seen clearly in the Results and Discussion section, as all the polarized and depolarized field correlation functions could be fitted to third-order Cumulant expression (22) with a good accuracy. Further, the fluorescence confocal laser scanning microscope pictures discussed in the next section reveals that different forms of *D. radiodurans* used in this study are nearly spherical. Hence Eqs. 5 and 6 can be approximated to

$$g^{(1)}_{\mathrm{VV}}(q,\tau) = A\exp(-\Gamma_{\mathrm{VV}}\tau) \quad (7)$$

and

$$g^{(1)}_{\mathrm{VH}}(q,\tau) = \exp(-\Gamma_{\mathrm{VH}}\tau) \quad (8)$$

with

$$\Gamma_{\mathrm{VV}} = D_{\mathrm{T}}q^2 \quad (9)$$

and

$$\Gamma_{\mathrm{VH}} = D_{\mathrm{T}}q^2 + 6D_{\mathrm{R}} \quad (10)$$

and

$$A = 45\alpha^2/(45\alpha^2+4\beta^2).$$

So polarized DLS experiments performed on our optically anisotropic, but nearly spherical in shape particles, sense mostly the translational diffusion, whereas the depolarized DLS experiments will have contributions from both the translational and rotational diffusion. In this case, the decay rate, Γ_{VH},is only amplitude modulated by the rotational diffusion coefficient (3,18,20,21). Equation 10 rests on the assumption that there is no coupling between translational and rotational motion. The validity of this assumption can be evaluated through the rotational-translational coupling parameter, $\gamma = q^2\Delta D_{\mathrm{T}}/D_{\mathrm{R}}$,, where $\Delta D_{\mathrm{T}}(= D_{\mathrm{II}} - D_{\perp}; D_{\mathrm{II}}$ and $D_{\perp}$ are the translational diffusion coefficient parallel and perpendicular to the rod's axis) is the anisotropy in the translational diffusion coefficient and $D_{\mathrm{R}}$is the rotational diffusion coefficient (20,21). Equation 10 is valid for small values of γ and for nearly spherical particles; γ is generally very small because $\Delta D_{\mathrm{T}}$is small.

The DLS and DDLS experiments were performed by placing the sample cell at the center of an optical vat filled with an index matching liquid (toluene) in the goniometer. The index matching liquid is used to suppress the reflection from the sample cell walls to the PMT. Experiments were performed at a constant temperature of 25 ± 0.1°C. The field correlation function,$g^{(1)}(q,\tau)$ was obtained from the measured ICF by using Eq. 2 and fitted to the third-order Cumulant expression (22) $\ln g^{(1)}(q,\tau) = -\Gamma\tau + \Gamma_2\tau^2/2! - \Gamma_3\tau^3/3! + \ldots$, to extract the decay rate, Γ, and polydispersity parameter, $P = (\Gamma_2/\Gamma^2)$ corresponding to particle size distribution.

RESULTS AND DISCUSSION

Fluorescence confocal laser scanning microscopy

One of the goals of this investigation is to grow different forms of *D. radiodurans* bacteria cells by controlling the nutrient concentration, and characterize their shape and size. The double-stranded DNA inside the *D. radiodurans* cells are tagged with the fluorescent dye molecule of acridine orange, which helps in imaging the cells using CLSM. Fig. 1, *a–c*, show the typical CLSM images containing several bacteria cell units with predominantly dimer, tetramer, and

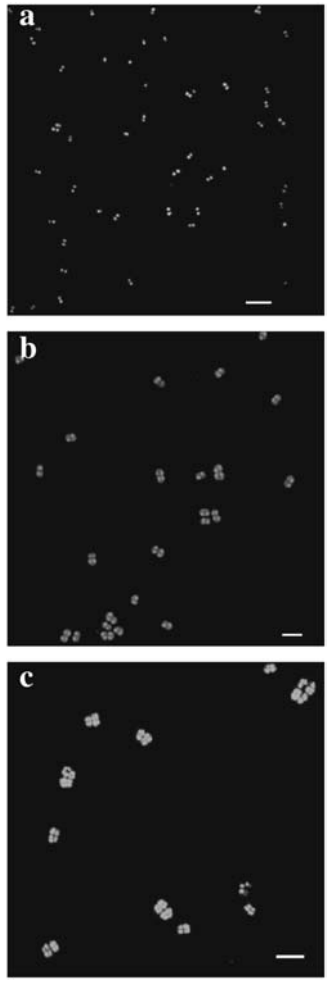

FIGURE 1 CLSM images of samples with predominantly (*a*) dimer, (*b*) tetramer, and (*c*) multimer of *D. radioduran* species. The images were taken using a 63×/1.2 numerical aperture water immersed objective lens and averaging over 40 frames. The scale bar is 5 μm.

multimer form of *D. radiodurans* species, respectively. The dimer and tetramer cells are found to be present in more than 90% in the respective samples, when the images were captured and analyzed over several frames. In the case of the multimer sample, tetramers in groups of four (16-cell cluster) were found to dominate in numbers in comparison to other combinations. All samples including the predominantly multimer sample are grown without the presence of any salt. This predominant culture of multimer form of *D. radiodurans* was achieved by controlling the nutrient concentration alone. However, in an earlier report by Chou et al. (23), the multimer form of *D. radiodurans* was grown by controlling the salt concentration. Cell lengths of dimer, tetramer, and multimer (16-cell cluster) form of *D. radiodurans* are obtained by performing image analysis on several frames containing predominantly dimers, tetramers, and multimers of *D. radiodurans*, respectively. Fig. 2, *a–c*, depict a single unit of dimer, tetramer, and multimer bacteria cell, respectively, imaged using 63×/1.2 numerical aperture water immersed objective lens. The aspect ratio (length/breadth) for dimer, tetramer, and multimer forms of *D. radiodurans* are obtained by image analysis on the monographs. The results obtained from CLSM studies are summarized in Table 1. These results were substantiated with light scattering data, which is presented in the following section.

Dynamic light scattering

The same batch of cultured samples with different forms of *D. radiodurans* was used for both polarized and depolarized DLS experiments, on which fluorescence CLSM measurements were performed. DLS experiments are quite susceptible to fine dust particles. Extreme care was taken to clean the *D. radiodurans* pellet obtained from the TGY media by thoroughly washing them with 0.22 μm filtered buffer of PBS. The washed pellet was directly resuspended into the light scattering cell with the same filtered buffer of PBS. Experiments were carried out on dilute solutions of *D. radiodurans*, so as to measure the self-diffusion coefficients of the species, while having enough number of cells in the scattering volume to have a proper statistics. ICFs for all the samples were accumulated both in the VV and VH scattering geometry for the scattering angles, $\theta = 20$–$50°$ with 5° interval, except at 50° for the live tetramer sample in the VH geometry, where the signal was very weak to measure.

The dynamic light-scattering technique can be effectively used to differentiate between motile and nonmotile living organisms (2). Brownian motion generally governs the motion of nonmotile organisms in dilute solutions, where the distance the organism travels before changing its direction due to collision with solvent molecules is much less than the probing length, q^{-1}. However, in the case of motile microorganisms, in addition to the Brownian motion, the organism can move in a particular direction up to a distance vt, where v is the speed of the organism. Generally, motile organisms tend to move in a particular direction for long distances, once they start moving. When the distance becomes much longer than q^{-1}, then its motion is no longer governed by Brownian motion alone. If the velocity, rather than Brownian motion, controls their movements, the scattered-field correlation function should depend on $q\tau$, whereas if Brownian motion alone controls their movements, the scattered field correlation function should depend on $q^2\tau$ (24,25). In the study presented here, the suspension concentrations were such that the mean free path is much larger compared to the probing length, q^{-1}, i.e., $\Lambda q \gg 1$. In Fig. 3, we have plotted the normalized scattered-field correlation function in the VV geometry as a function of time at different scattering angles, $\theta = 20$–$50°$ for the live dimer species. It is observed from the figure that the scattered-field correlation function for higher angles relaxes faster than those for lower angles. In Fig. 4, the same data is replotted as a function of $q^2\tau$. This shows a complete collapse of scattered-field correlation function measured at all the angles, indicating that Brownian motion solely governs the movements of dimer cells in dilute solutions. This result corroborates with the microscopy study (26) wherein the live organism of *D. radiodurans* is observed to be nonmotile in nature. Similar results are observed for the live tetramer and multimer forms of *D. radiodurans*. Henceforth, all the transport properties of *D. radiodurans* are analyzed, as Brownian motion is the only mechanism that governs their movements.

Fig. 5 represents the normalized field correlation function in the VV geometry for predominantly live dimer, tetramer, and multimer forms of *D. radiodurans* at the scattering angle, $\theta = 50°$. This shows that the correlation function for dimer species decays faster than that for tetramer species,

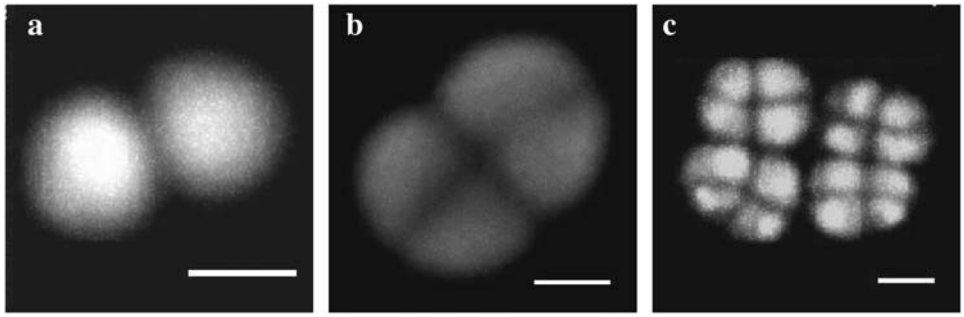

FIGURE 2 CLSM images of single (*a*) dimer, (*b*) tetramer, and (*c*) multimer of *D. radiodurans* species. The images were taken using a 63×/1.2 numerical aperture water immersed objective lens and averaging over 40 frames. The scale bar is 1 μm.

which in turn decays faster than that for multimer species. This type of behavior is a consequence of the dimer cell being smaller in size compared to the tetramer cell, which in turn is smaller when compared to the multimer cell. Measurements performed at different scattering angles (not shown here) showed similar results. Normalized field correlation functions for all the samples were fitted to a good accuracy to third order Cumulant expression (22). From the analysis, polydispersity values ranging between 0.1 and 0.15 are obtained for the predominantly dimer, tetramer, and multimer form of *D. radiodurans* samples. This low value of polydispersity index suggests each sample is chiefly populated with the same form of *D. radiodurans* only. The DLS results are in accordance with the CLSM observations.

Fig. 6 shows the variation of the decay rate in the VV geometry, Γ_{VV}, as function of q^2 for the live dimer, tetramer, and multimer forms of *D. radiodurans*. A linear fit to the curves results in a slope of $2.12 \pm 0.024 \times 10^{-9}$ cm^2/s, $1.97 \pm 0.015 \times 10^{-9}$ cm^2/s, and $1.21 \pm 0.013 \times 10^{-9}$ cm^2/s for the dimer, tetramer, and multimer form of *D. radiodurans*, respectively, and all the lines pass through the origin. According to Eq. 9, the slope of these lines is equal to the average translational diffusion coefficient, D_T, for the respective forms. From the measured average translational diffusion coefficient, the bacteria cell size can be calculated using Stokes-Einstein relation (27)

$$D_T = \frac{k_B T}{3\pi\eta d_H}, \tag{11}$$

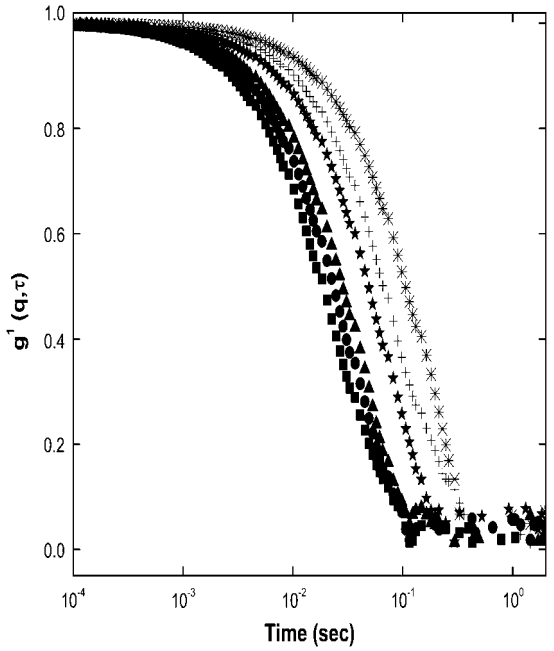

FIGURE 3 Normalized field autocorrelation function of *D. radiodurans* dimer species measured in the polarized (VV) geometry at scattering angles $\theta = 20°$ (∗), 25° (+), 30° (★), 40° (▲), 45° (●), and 50° (■).

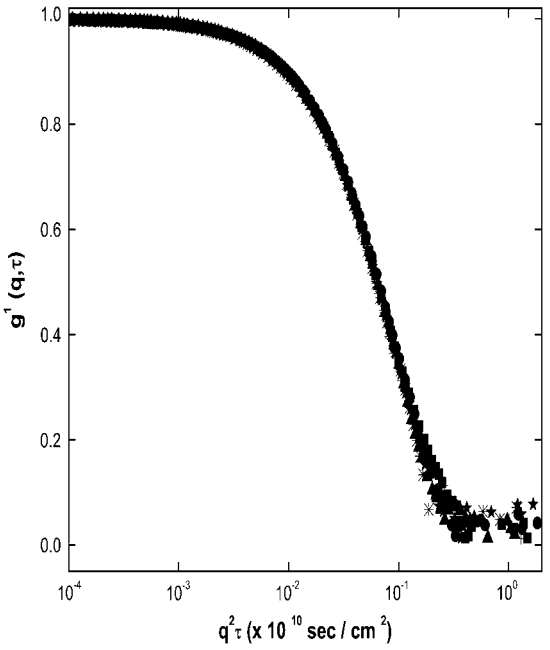

FIGURE 4 Normalized field autocorrelation function of *D. radiodurans* dimer species measured in the polarized (VV) geometry at scattering angles $\theta = 20°$ (∗), 25° (+), 30° (★), 40° (▲), 45° (●), and 50° (■), plotted against $q^2\tau$. All the curves measured at different scattering angles collapse into each other.

where k_B is the Boltzmann constant, T is the temperature in kelvin, η is the viscosity of the medium, and d_H is the particle hydrodynamic diameter. The average cell size of dimer, tetramer, and multimer form of *D. radiodurans* obtained using Eq. 12 is presented in Table 1. The Stokes-Einstein equation was used to calculate the cell sizes, because all forms of *D. radiodurans* cells, i.e., dimer, tetramer, and multimer were of low aspect ratio (see Table 1), and can be treated as spherical particles. The cell size obtained from the polarized DLS experiments are found to be in good agreement with the corresponding length obtained from the CLSM study. The large size of 3.61 μm obtained for the predominantly multimer sample compared to 2.05 μm obtained for the predominantly dimer sample from polarized DLS experiments confirms that the CLSM image of the multimer form of *D. radiodurans* (Fig. 1 *c*) is for real, and not due to any artifacts of clumping of dimer or tetramer species during the spreading of the samples on to the glass slide. The inset of Fig. 6 shows the average size of dimer, tetramer, and multimer form of *D. radiodurans* as a function of the scattering angle, θ. This independence of average size with θ suggests that there is no interaction among the species.

Depolarized dynamic light scattering

Optically or geometrically anisotropic particles depolarize the incident light. The strength of the depolarized scattering

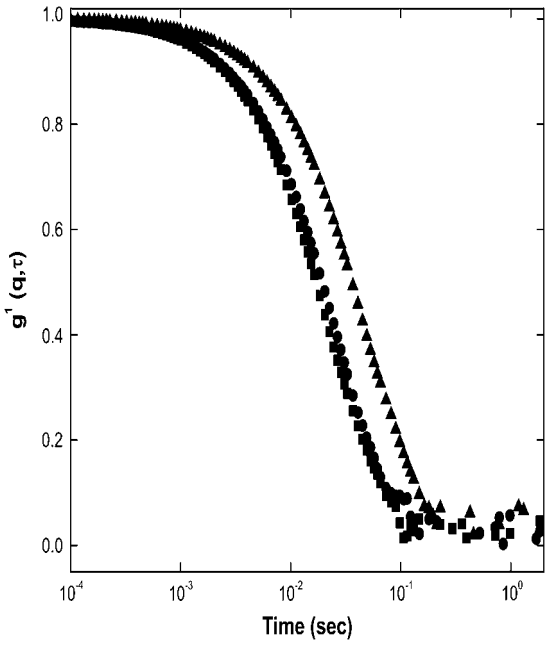

FIGURE 5 Normalized field autocorrelation function for the dimer (■), tetramer (●), and multimer (▲) form of *D. radiodurans* measured in the polarized (VV) geometry at a scattering angle $\theta = 50°$.

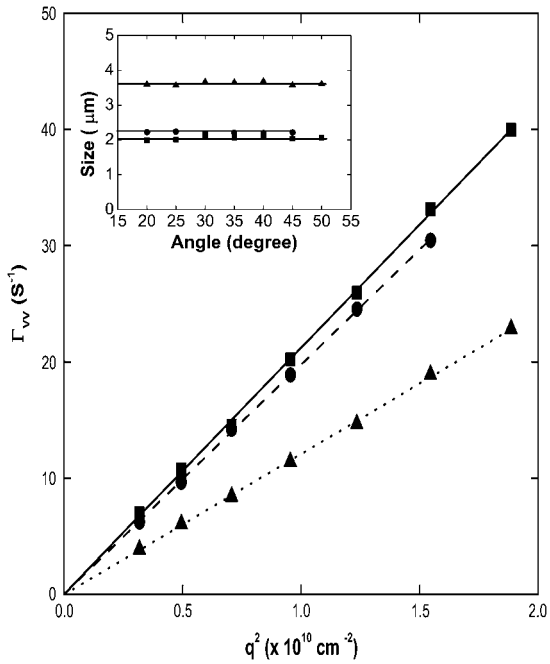

FIGURE 6 Dependence of the polarized decay rates, Γ_{VV}, on the square of the scattering wave vector q^2 for the dimer (■), tetramer (●), and multimer *D. radiodurans* (▲) species. Inset shows the average sizes of dimer, tetramer, and multimer species as a function of the scattering angles.

signal depends on the optical anisotropy of the particles building blocks (2). Generally, the depolarized signal is so weak that it is a very tedious and time-consuming experiment to perform. In the study presented here, we have carried out depolarized DLS experiments on both predominantly dimer and tetramer forms of *D. radiodurans* samples. We observed a small but finite measurable depolarized signal. The depolarized signal is very weak, particularly for higher angles and because of this the total experimental accumulation time was as high as 45–60 min to get proper photon statistics. Fig. 7 shows the field correlation function for the predominantly live dimer species both in the VV and VH geometry at the scattering angle, $\theta = 50°$. The correlation function for the VH geometry relaxes faster than that for the VV geometry. This implies that a depolarized DLS experiment, which measures both the rotational and translational diffusion coefficient, occurs in a faster timescale compared to a polarized DLS experiment, which measures only the translational diffusion coefficient.

Fig. 8 represents the decay rates in VH geometry, Γ_{VH}, for predominantly live dimer and tetramer species as a function of q^2. The linear dependence of Γ_{VH} with q^2 suggests a decoupling between rotational and translational motion. Linear fits to both the curves result in a slope and an intercept of $2.08 \pm 0.02 \times 10^{-9}$ cm^2/s and 1.09/s and $1.94 \pm 0.026 \times 10^{-9}$ cm^2/s and 0.587/s for the predominantly live dimer and tetramer species, respectively. The slope of the curve is equal to the average translational diffusion coefficient, D_T, and the intercept is proportional to the rotational diffusion coefficient, D_R, according to Eq. 10. It can be seen that the average translational diffusion coefficients obtained using depolarized DLS experiments is the same as that obtained in the polarized

TABLE 1 Size distribution of different forms of *D. radiodurans* bacteria cells as obtained from the polarized and depolarized DLS and CLSM measurements

	CLSM		DLS		
			Polarized	Depolarized	
D. radiodurans form	L (μm)	Aspect Ratio	$d_h(\mu m)/D_T$*	$d_h(\mu m)/D_T$†	$d_h(\mu m)/D_R$‡
Dimer	1.86 ± 0.09	1.7	2.06 ± 0.023	2.09 ± 0.02	1.92
Tetramer	2.11 ± 0.08	1.4	2.22 ± 0.017	2.25 ± 0.03	2.37
Multimer	3.45 ± 0.14	1.35	3.61 ± 0.039	(–)	(–)

*d_h is calculated using Eqs. 9 and 11.
†d_h is calculated using Eqs. 10 and 11.
‡d_h is calculated using Eqs. 10 and 12.

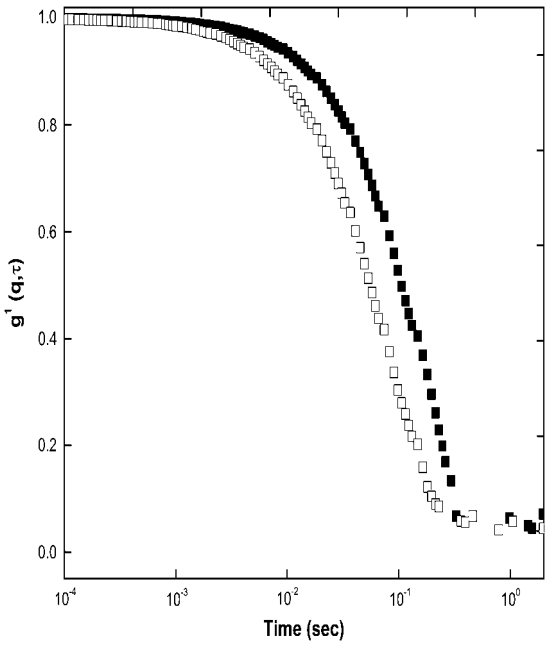

FIGURE 7 Normalized field autocorrelation function of *D. radiodurans* dimer species measured in the polarized (VV) (■) and depolarized (VH) (□) geometry at the scattering angle $\theta = 50°$.

DLS experiments. From the *y*-intercept, a very small rotational diffusion coefficient of 0.182/s for the live dimer species and an even smaller rotational diffusion coefficient of 0.098/s for the live tetramer species are obtained. This small rotational diffusion coefficient is due to the large cell size of the dimer and tetramer forms of *D. radiodurans*. We failed to measure any noticeable rotational diffusion coefficient for the multimer form of *D. radiodurans*, which could be due to a larger average size and a smaller size anisotropy compared to the dimer and tetramer forms of *D. radiodurans*. From the average rotational diffusion coefficient measured using depolarized DLS experiments, the bacteria cell size can be calculated using the Stokes-Einstein-Debye relation given by (27)

$$D = \frac{k_B T}{\pi \eta d_H^3}. \tag{12}$$

From the depolarized DLS experiments, an average cell size of 1.92 and 2.37 μm are obtained from the measured rotational diffusion coefficient (using Eq. 12) compared to 2.09 and 2.25 μm obtained from the measured translational diffusion coefficient (using Eq. 11) for the dimer and tetramer forms of *D. radiodurans*, respectively. The cell size obtained from the translational diffusion coefficient measured independently with polarized and depolarized DLS experiments are essentially the same. All the size information for the dimer, tetramer, and multimer forms of *D. radiodurans* obtained from CLSM and polarized and depolarized DLS experiments are presented in Table 1 for comparison.

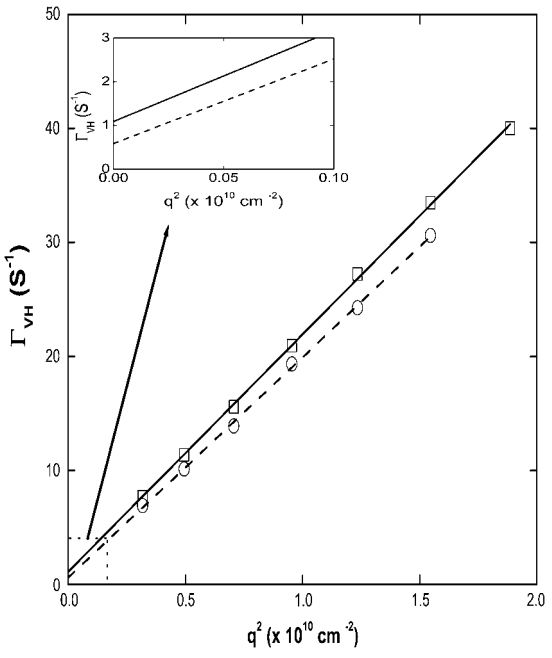

FIGURE 8 Dependence of the depolarized decay rates, Γ_{VH}, on the square of the scattering wave vector q^2 for dimer (□) and tetramer *D. radiodurans* (○) species. The inset shows the expanded version of the dotted portion showing the *y*-intercept clearly.

Difference between live and dead cells of *D. radiodurans*

Dilute solutions of predominantly live dimer and tetramer bacteria cells used for DLS experiments were stored at 4°C for 1 month without providing any nutrition in a buffered solution. After 1 month, the survivability of the cells was checked by staining them with a live/dead stain (Molecular Probes). By this dual staining technique, it was confirmed that the month-old *D. radiodurans* cells are dead because of the lack of nutrition. Both the polarized and depolarized DLS experiments were performed on the dead samples to find out whether the DLS technique is capable of differentiating between live and dead *D. radiodurans*. Fig. 9 shows the decay constants, Γ_{VV}, for the predominantly dead and live dimer and tetramer cells plotted as a function of q^2. For clarity, data have been plotted only up to the scattering angle, $\theta = 35°$. Linear fits to the curves results in a slope of $2.21 \pm 0.02 \times 10^{-9}$ cm^2/s and $2.07 \pm 0.01 \times 10^{-9}$ cm^2/s for the predominantly dead dimer and tetramer cells, respectively, and both the lines pass through the origin. Fig. 10 represents the decay rates, Γ_{VH}, for the dead and live dimer and tetramer cells as a function of q^2. Linear fits to the curves for the dead dimer and tetramer cells samples yield a slope and intercept of $2.16 \pm 0.016 \times 10^{-9}$ cm^2/s and 1.13/s and $2.01 \pm 0.02 \times 10^{-9}$ cm^2/s and 0.59/s, respectively. Similar to the VV geometry, data have been plotted only up to the scattering angle, $\theta = 35°$. The rotational diffusion coefficient for the dead dimer and tetramer cells is practically the same when compared to the live dimer and tetramer cells. Similar to the

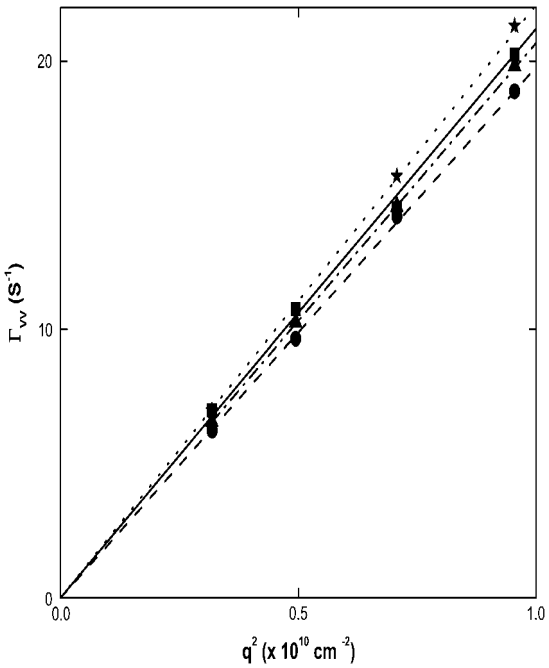

FIGURE 9 Dependence of the polarized decay rates, Γ_{VV}, on the square of the scattering wave vector q^2 for live (■) and dead (★) dimer *D. radiodurans* and live (●) and dead (▲) tetramer *D. radiodurans* species.

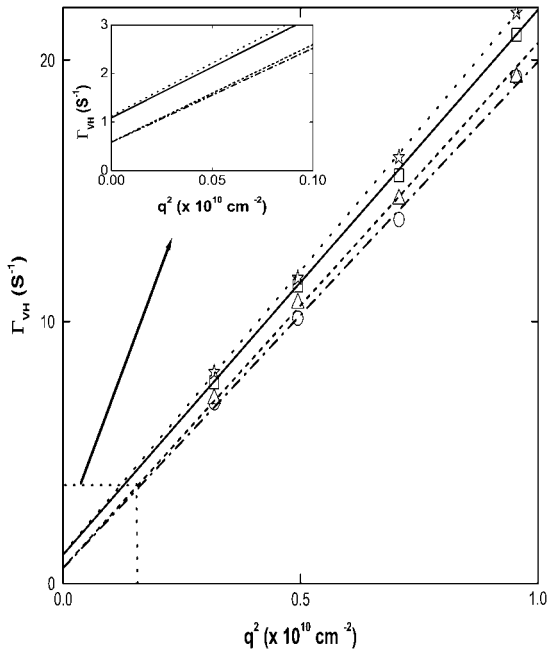

FIGURE 10 Dependence of the depolarized decay rates, Γ_{VH}, on the square of the scattering wave vector q^2 for live (□) and dead (☆) dimer *D. radiodurans* and live (○) and dead (△) tetramer *D. radiodurans* species. The inset shows the expanded version of the dotted portion showing the *y*-intercept clearly.

live *D. radiodurans* samples, the translational diffusion coefficient measured for the dead samples using polarized and depolarized DLS experiments is essentially the same. The average size obtained for the dead dimer and tetramer cells from the translational diffusion coefficient using Eq. 11 is 1.97 ± 0.018 μm and 2.1 ± 0.01 μm, respectively. This is slightly smaller in size compared to the corresponding live cells (see Table 1). This could be due to shrinkage of cells due to the lack of nutrition/starvation.

CONCLUSIONS

D. radiodurans samples with predominantly dimer, tetramer, and multimer forms were cultured under controlled growth conditions. The different forms of *D. radiodurans* cultured, under controlled growth conditions, were confirmed using the fluorescence CLSM imaging technique. We have used both the polarized and depolarized DLS experiments to study the rotational and translational dynamics of these grown cultures. The translational diffusion coefficients for the dimer and tetramer forms of *D. radiodurans*, measured using polarized and depolarized DLS experiments, match very well with each other. The depolarized DLS experiments give a very small rotational diffusion coefficient for the dimer and even smaller rotational diffusion coefficient for the tetramer forms of *D. radiodurans*, whereas no noticeable rotational diffusion coefficient for multimer form of *D. radiodurans* was observed. The average size obtained from the polarized DLS measurements for the dimer, tetramer, and multimer forms of *D. radiodurans* are in accordance with that obtained by fluorescence CLSM. The *D. radiodurans* microorganism is confirmed to be nonmotile using DLS experiments. The size of dead cells of *D. radiodurans* is found to be marginally smaller than the corresponding live cells size. However, no additional differences between the dead and live cells could be observed from the polarized and depolarized DLS experiments.

The authors thank Dr. B. Purniah for careful reading of the manuscript and helpful suggestions.

REFERENCES

1. Steer, M. W. 1983. Application of laser light scattering to biological systems. *In* The Application of Laser Light Scattering to the Study of Biological Motion. NATO ASI Series, Vol. 59. J. C. Earnshaw and M. W. Steer, editors. Plenum Press, New York. 43–49.
2. Berne, B., and R. Pecora. 1981. Dynamic Light Scattering: With Applications to Chemistry, Biology and Physics. John Wiley & Sons, New York.
3. Zero, K., and R. Pecora. 1985. Dynamic depolarized light scattering. *In* Dynamic Light Scattering: Application of Photon Correlation Spectroscopy. R. Pecora, editor. Plenum Press, New York. 59–81.
4. Riley, R. G., and J. M. Zachara. 1992. Chemical Contaminants on DOE Lands and Selection of Contaminant Mixtures for Subsurface Science Research. U.S. Department of Energy Office of Energy Research Subsurface Science Program, Washington, D.C.
5. MaCilwain, C. 1996. Science seeks weapons clean-up role. *Nature*. 383:375–379.
6. McCullough, J., T. C. Hazen, S. M. Benson, F. Blaine-Metting, and A. C. Palmisano. 1999. Bioremediation of metals and radionuclides.

U.S Department of Energy Office of Biological and Environmental Research, Germantown, MD.

7. Daly, M. J., and K. Minton. 1995. Resistance to radiation. *Science*. 270:1318.
8. Battista, J. R. 1997. Against all odds: the survival strategies of *Deinococcus radiodurans*. *Annu. Rev. Microbiol*. 51:203–224.
9. Masters, C. I., R. G. Murray, B. E. Moseley, and K. W. Minton. 1991. DNA polymorphisms in new isolates of *Deinococcus radiodurans*. *J. Gen. Microbiol*. 137:1459–1469.
10. Counsell, T. J., and R. G. E. Murray. 1986. Polar lipid profiles of the genus *Deinococcus*. *Int. J. Syst. Bacteriol*. 36:202–206.
11. Lange, C. C., L. P. Wackett, K. W. Minton, and M. J. Daly. 1998. Engineering a recombinant *Deinococcus radiodurans* for organopollutant degradation in radioactive mixed waste environments. *Nat. Biotechnol*. 16:929–933.
12. Battista, J. R., A. M. Earl, and M. J. Park. 1999. Why is *Deinococcus radiodurans* so resistant to ionizing radiation? *Trends Microbiol*. 7:362–365.
13. Levin-Zaidman, S., J. Englander, E. Shimon, A. K. Sharma, K. W. Minton, and A. Minsky. 2003. Ringlike structure of the *Deinococcus radiodurans* genome: A key to radioresistance? *Science*. 299:254–256.
14. Murray, R. G., M. Hall, and B. J. Thompson. 1983. Cell division in *Deinococcus radiodurans* and a method for displaying septa. *Can. J. Microbiol*. 29:1412–1423.
15. Sheppard, C. J. R., and D. M. Shotton. 1997. Confocal Laser scanning Microscopy. BIOS Scientific Publishers, Springer-Verlag, New York.
16. Venkateswaran, A., S. C. McFarlan, D. Ghosal, K. W. Minton, A. Vasilenko, K. Makarova, L. P. Wackett, and M. J. Daly. 2000. Physiologic determinants of radiation resistance in *Deinococcus radiodurans*. *Appl. Environ. Microbiol*. 6:2620–2626.
17. Siegert, A. J. 1942. Massachusetts Institute of Technology Radiation Laboratory Report.
18. Diaz-Leyva, P., E. Perez, and J. L. Arauz-Lara. 2004. Dynamic light scattering by optically anisotropic colloidal particles in polyacrylamide gels. *J. Chem. Phys*. 121:9103–9110.
19. De Souza Lima, M. M., J. T. Wong, M. Paillet, R. Borsali, and R. Pecora. 2003. Translational and rotational dynamics of rodlike cellulose whiskers. *Langmuir*. 19:24–29.
20. Cush, R., P. S. Russo, Z. Kucukyavuz, Z. Bu, D. Neau, D. Shih, S. Kucukyavuz, and H. Ricks. 1997. Rotational and translational diffusion of a rodlike virus in random coil polymer solutions. *Macromolecules*. 30:4920–4926.
21. Cush, R., D. Dorman, and P. S. Russo. 2004. Rotational and translational diffusion of tobacco mosaic virus in extended and globular polymer solutions. *Macromolecules*. 37:9577–9584.
22. Koppel, D. E. 1972. Analysis of macromolecular polydiversity in intensity correlation spectroscopy: The method of Cumulants. *J. Chem. Phys*. 57:4814–4820.
23. Chou, F. I., and S. T. Tan. 1991. Salt-mediated multicell formation in *Deinococcus radiodurans*. *J. Bacteriol*. 173:3184–3190.
24. Nosal, R., S. H. Chen, and C. C. Lai. 1971. Use of laser scattering for quantitative determinations of bacterial motility. *Opt. Commun*. 4:35–39.
25. Nosal, R., and S. H. Chen. 1972. Light scattering data from motile bacteria. *J. Phys*. (*Paris*)(Suppl.) 33:C1–171.
26. Anderson, A., H. Nordan, R. Cain, G. Parish, and D. Duggan. 1956. Studies on radioresistant micrococcus, isolation, morphology, cultural characteristics and the resistance to gamma radiation. *Food Technol*. 10:577–578.
27. Einstein, A. 1956. Investigations on the Theory of the Brownian Movement. Dover, NY.